Parasitology International 86 (2022) 102479

Contents lists available at ScienceDirect

Parasitology International

journal homepage: www.elsevier.com/locate/parint

Research paper

Distinct effects on the secretion of MTRAP and AMA1 in *Plasmodium yoelii* following deletion of acylated pleckstrin homology domain-containing protein

Nattawat Chaiyawong [a,b], Takahiro Ishizaki [a,b,c], Hassan Hakimi [b,d], Masahito Asada [a,b,e], Kazuhide Yahata [b], Osamu Kaneko [a,b,*]

[a] Program for Nurturing Global Leaders in Tropical and Emerging Communicable Diseases, Graduate School of Biomedical Sciences, Nagasaki University, 1-12-4 Sakamoto, Nagasaki 852-8523, Japan
[b] Department of Protozoology, Institute of Tropical Medicine (NEKKEN), Nagasaki University, 1-12-4 Sakamoto, Nagasaki 852-8523, Japan
[c] Laboratory for Molecular Infection Medicine Sweden, Department of Molecular Biology, Umeå University, Umeå 901 87, Sweden
[d] Department of Veterinary Pathobiology, College of Veterinary Medicine, Texas A&M University, College Station, TX 77843, United States
[e] National Research Center for Protozoan Diseases, Obihiro University of Agriculture and Veterinary Medicine, Nishi 2-11, Obihiro, Hokkaido 080-0834, Japan

ARTICLE INFO

Keywords:
Erythrocyte invasion
Exocytosis
Malaria
Microneme
PH-domain containing protein

ABSTRACT

Plasmodium, the causative agents of malaria, are obligate intracellular organisms. In humans, pathogenesis is caused by the blood stage parasite, which multiplies within erythrocytes, thus erythrocyte invasion is an essential developmental step. Merozoite form parasites released into the blood stream coordinately secrets a panel of proteins from the microneme secretory organelles for gliding motility, establishment of a tight junction with a target naive erythrocyte, and subsequent internalization. A protein identified in *Toxoplasma gondii* facilitates microneme fusion with the plasma membrane for exocytosis; namely, acylated pleckstrin homology domain-containing protein (APH). To obtain insight into the differential microneme discharge by malaria parasites, in this study we analyzed the consequences of APH deletion in the rodent malaria model, *Plasmodium yoelii*, using a DiCre-based inducible knockout method. We found that APH deletion resulted in a reduction in parasite asexual growth and erythrocyte invasion, with some parasites retaining the ability to invade and grow without APH. APH deletion impaired the secretion of microneme proteins, MTRAP and AMA1, and upon contact with erythrocytes the secretion of MTRAP, but not AMA1, was observed. APH-deleted merozoites were able to attach to and deform erythrocytes, consistent with the observed MTRAP secretion. Tight junctions were formed, but echinocytosis after merozoite internalization into erythrocytes was significantly reduced, consistent with the observed absence of AMA1 secretion. Together with our observation that APH largely colocalized with MTRAP, but less with AMA1, we propose that APH is directly involved in MTRAP secretion; whereas any role of APH in AMA1 secretion is indirect in *Plasmodium*.

1. Introduction

Plasmodium protozoan parasites are the causative agents of malaria, a life-threatening disease with 229 million malaria cases and 409,000 deaths in 2019 [1]. *Plasmodium* spp. belong to the phylum Apicomplexa, whose members are largely obligate intracellular parasites. For human malaria, clinical manifestation of infection and pathogenesis is due to asexual stage proliferation within erythrocytes; and erythrocyte invasion is an essential step for *Plasmodium* blood stage development. This process consists of several specific molecular interactions between the merozoite form parasite and the host erythrocyte [2–4]. After initial attachment of the merozoite to the erythrocyte, the merozoite reorients and deforms the erythrocyte to establish an irreversible tight junction between the parasite anterior end and the erythrocyte membrane. During these steps, one or more thrombospondin-related anonymous protein (TRAP) family proteins are likely responsible for the erythrocyte

* Corresponding author at: Department of Protozoology, Institute of Tropical Medicine (NEKKEN), Nagasaki University, 1-12-4 Sakamoto, Nagasaki 852-8523, Japan.
E-mail addresses: takahiro.ishizaki@umu.se (T. Ishizaki), masada@obihiro.ac.jp (M. Asada), kyahata@nagasaki-u.ac.jp (K. Yahata), okaneko@nagasaki-u.ac.jp (O. Kaneko).

https://doi.org/10.1016/j.parint.2021.102479
Received 19 September 2021; Received in revised form 29 September 2021; Accepted 4 October 2021
Available online 7 October 2021

deformation, mediated through merozoite gliding motility [5]. Additionally, reticulocyte-binding-like (RBL or Rh) proteins were proposed to be involved in the target cell selection [6], and erythrocyte-binding-like (EBL) proteins are responsible for the tight junction formation [7,8]. The merozoite actively internalizes into an erythrocyte, mediated by the parasite actomyosin motor machinery using a scaffold structure between the merozoite and the erythrocyte membrane, called a moving junction. The moving junction is formed by an interaction between apical membrane antigen 1 (AMA1) on the merozoite surface and rhoptry neck protein (RON) complex proteins that are inserted to the erythrocyte membrane - a model in part based on observations in *T. gondii* [9,10]. The posterior movement of this junction drives merozoite entry into the nascently formed parasitophorous vacuole in the erythrocyte [11]. The invaded erythrocyte undergoes echinocytosis, a minutes long deformation of the erythrocyte with the appearance of transient spike-like extrusions of the surface membrane [12,13].

Secretion of microneme proteins, such as TRAP, EBL, and AMA1, are regulated by a sequence of signaling events involving kinases, lipids, and calcium [14]. According to a model largely generated by characterization of *T. gondii* MIC2 (a homolog of *Plasmodium* TRAP proteins) and AMA1, diacylglycerol is produced during a signaling cascade involving phospholipase C. The diacylglycerol is further converted to phosphatidic acid (PA) by a diacylglycerol kinase on the inner leaflet of the plasma membrane, which is then recognized by acylated pleckstrin homology (pH) domain-containing protein (APH) on the cytosolic face of the microneme membrane. The binding of APH to PA facilitates juxtaposition of these two membranes, to release the contents of micronemes [15,16]. A double C2 domain protein, DOC2.1, was reported to be responsible for microneme membrane fusion in *T. gondii* and *Plasmodium falciparum* [17]. Compared to TRAP/MIC2 and AMA1, for which homologs are found among all apicomplexan parasites, RBL and EBL are only found in *Plasmodium* spp. In *P. falciparum*, RH1, an RBL family member, is required for the secretion of EBA175, an EBL family member [18]. A pleckstrin homology domain-containing protein, PH2, was proposed to be involved in EBA175 secretion, and this protein showed higher binding activities to phosphoinositides than PA and is not involved in AMA1 secretion [19]. Thus, two signaling cascades appear to control the exocytosis of microneme vesicles.

T. gondii APH (TgAPH) colocalizes with the microneme proteins MIC2, MIC4, and MIC6, and its trafficking is regulated *via* N-terminal palmitoylation and myristoylation [20]. Conditional knockdown of TgAPH resulted in pronounced defects in both parasite egress and invasion. TgAPH-knockdown parasites also exhibited a defect in secretion of MIC2 and another microneme protein, AMA1, but did not alter microneme biogenesis, localization, and intracellular growth. Specific interaction with PA was shown for recombinant TgAPH as well as recombinant *P. falciparum* APH. Because APH is conserved across Apicomplexa, a similar role is expected for malaria parasites [20]. However, the erythrocyte invasive merozoite stage of malaria parasites has unique features absent in *T. gondii*; for example, only *Plasmodium* merozoites possess EBL and RBL protein families, and *Plasmodium* egress is not controlled by microneme proteins [21].

Rodent malaria parasite models offer ease in laboratory maintenance and experimental genetic modifications. In the previous study, we reported *Plasmodium yoelii* required several minutes after egress for merozoites to invade erythrocytes [2]. Based on this unique feature, we developed methods to purify *P. yoelii* merozoites retaining competency to invade erythrocytes for more than 4 h [22] and to capture a large number of erythrocyte invasion events by video time-lapse video imaging for 40 min [8]. Utilizing these research resources, in this study, we investigated the roles of APH in malaria parasites by analyzing transgenic *P. yoelii* 17×L lines in which the *aph* gene locus (PY17×_0716800) was conditionally excised using the dimerisable Cre-recombinase (DiCre)-loxP system [23].

2. Materials and methods

2.1. Parasites and animals

DiCre-expressing *P. yoelii* 17XL (17X-DiCre) and PyPKAc-iKO parasites were generated previously [23]. *P. yoelii* parasites were maintained through inoculation of 6–8-week-old ICR or BALB/c female mice (Japan SLC, Hamamatsu, Japan). All animal studies were performed under the approval of the Animal Care and Use Committee of Nagasaki University.

2.2. Plasmid construction

To construct the pDC2-Cas9-PyU6-PyAPH-3'loxP-hDHFR/yFCU plasmid, the pDC2-cam-Cas9-PyU6-hDHFR plasmid [23] was digested with *Bbs*I and ligated with a DNA fragment containing a gRNA1 component targeting the *P. yoelii aph* gene locus (PY17X_0716800). The *aph* gene locus was amplified from *P. yoelii* 17XL genomic DNA (gDNA) with primers P18 and P19 using an In-Fusion HD cloning kit (Takara Bio Inc., Shiga, Japan). Then, a DNA fragment containing a sequence encoding the 5′ homologous region (HR1) of the *aph* gene locus followed by Myc epitopes and a DNA fragment containing a loxP sequence and 3' HR (HR2) of the *aph* gene locus were PCR-amplified from *P. yoelii* 17XL gDNA using primers P20 and P21 or P24 and P25, respectively, then ligated using the In-Fusion method with the above plasmid digested with *Hpa*I and *Aat*II. The generated plasmid was digested with *Not*I and ligated using the In-Fusion method with a DNA fragment containing an hDHFR/yFCU expression cassette amplified from the pDC2-Cas9-PyU6-PypPK1-Myc [24] plasmid with P22 and P23. Parasite gDNA was extracted using a QIAamp DNA blood mini kit (Qiagen, Hilden, Germany).

To construct the pDC2-Cas9-PyU6-PyAPH-5'loxPi plasmid, pDC2-cam-Cas9-PyU6-hDHFR plasmid was digested with *Bbs*I and ligated with a DNA fragment containing the gRNA2 component targeting the *aph* gene locus and amplified from *P. yoelii* 17XL gDNA with primers P26 and P27 using an In-Fusion HD cloning kit. Then, HR3 and HR4 were amplified from parasite gDNA with primers P28 and P29 or P30 and P31, respectively. LoxP-intron sequence (103 bp) and a *Not*I site were added to primers P30 and P31, respectively, for HR4 [25]. The gRNA2-inserted plasmid was digested with *Hpa*I and *Aat*II and the HR3 and HR4 fragments were inserted using the In-Fusion method. The resulting plasmid was digested with NotI and a DNA fragment containing hDHFR/yFCU expression cassette amplified with P32 and P33 was then inserted as described.

To construct the pDC2-Cas9-PyU6-PyMTRAP-Ty plasmid, the pDC2-cam-Cas9-PyU6-hDHFR plasmid was digested with *Bbs*I and ligated with a DNA fragment containing the gRNA3 component targeting the *mtrap* gene locus. The *mtrap* gene locus was amplified from *P. yoelii* 17XL gDNA with primers P34 and P35 using an In-Fusion HD cloning kit. Then, the HR5 with a sequence coding for a Ty epitope and HR6 were amplified from parasite gDNA with primers P36 and P37 or P40 and P41, respectively. The gRNA3-inserted plasmid was digested with *Hpa*I and *Aat*II and these two DNA fragments were inserted using the In-Fusion method. A DNA fragment containing an hDHFR/yFCU expression cassette was amplified with P38 and P39 and ligated with the above *Not*I-digested plasmid. All primers used to generate plasmids are shown in the supplemental Table S1. The plasmids for transfection were prepared using a HiSpeed Plasmid Midi Kit (Qiagen, Hilden, Germany).

2.3. Generation of transgenic parasite lines

Firstly, the 3′ side of the *aph* gene locus of a *P. yoelii* 17XL-based parasite cloned line expressing DiCre recombinase [23] was modified using the CRISPR/Cas9 genome editing method using the plasmid pDC2-Cas9-PyU6-PyAPH-3'loxP-hDHFR/yFCU to yield two APH-3'loxP pre-5FC parasite lines. To remove the hDHFR/yFCU expression cassette from the parasite genome, negative selection was done by oral

administration of 5-fluorocytosine (5FC; Sigma-Aldrich, St. Louis, Missouri, USA) *via* drinking water (1 mg/mL) to yield 2 APH-3'loxP parasite lines [26]. After cloning, the 5′ side of the *aph* gene locus of two APH-3'loxP cloned parasite lines was further modified using a plasmid pDC2-Cas9-PyU6-PyAPH-5'loxPi, the hDHFR/yFCU expression cassette was removed as above, and then cloning was performed to yield PyAPH-iKO clones #1 and #2. PyAPH-iKO clone #1 was further modified to tag its PyMTRAP with a Ty epitope using the plasmid pDC2-Cas9-PyU6-PyMTRAP-Ty.

Transfection to *P. yoelii* was performed as described with minor modifications [8]. Schizonts were enriched by density gradient centrifugation using Nycodenz solution (1.077 g/mL) and were mixed with human T cell nucleofector solution (Lonza, Basel, Switzerland) containing 20 μg of circular plasmids and electroporated using a Nucleofector™ 2b device (Lonza; U-33 program). Drinking water containing 0.07 g/mL pyrimethamine (Fukuzyu Pharmaceutical Co., LTD, Toyama, Japan) was administrated orally beginning 1 day post transfection and parasites emerged following drug selection were passaged to a new mouse, then cloned by limiting dilution. To confirm the modification of the target gene locus, gDNA of transfectants were extracted using a QIAamp DNA Blood Mini Kit (Qiagen), and PCR with specific diagnostic primer pairs (Table S1) and Southern blot analysis were performed.

2.4. Southern blotting

Ten micrograms of parasite gDNA was digested with *Hpa*I and *Eco*RI for probe 1 amplified with primers P10 and P11 from parasite gDNA or *Nde*I and *Sca*I for probe 2 amplified with primers P12 and P13 using plasmid as template (Fig. 1). The pDC2-Cas9-PyU6-PyAPH-5'loxPi plasmid digested with ApaI and *Kpn*I was used as a control. Digested DNA was loaded onto an agarose gel for electrophoresis and transferred to HyBond N+ membrane (GE Healthcare, Buckinghamshire, U.K.). Probes were labeled and hybridized using an AlkPhos Direct kit (GE Healthcare) and chemiluminescent signals from CDP-star (GE Healthcare) was detected by a multipurpose charge-coupled-device (CCD) camera system (LAS-4000 mini; Fujifilm, Tokyo, Japan) with Multi Gauge software (Fujifilm).

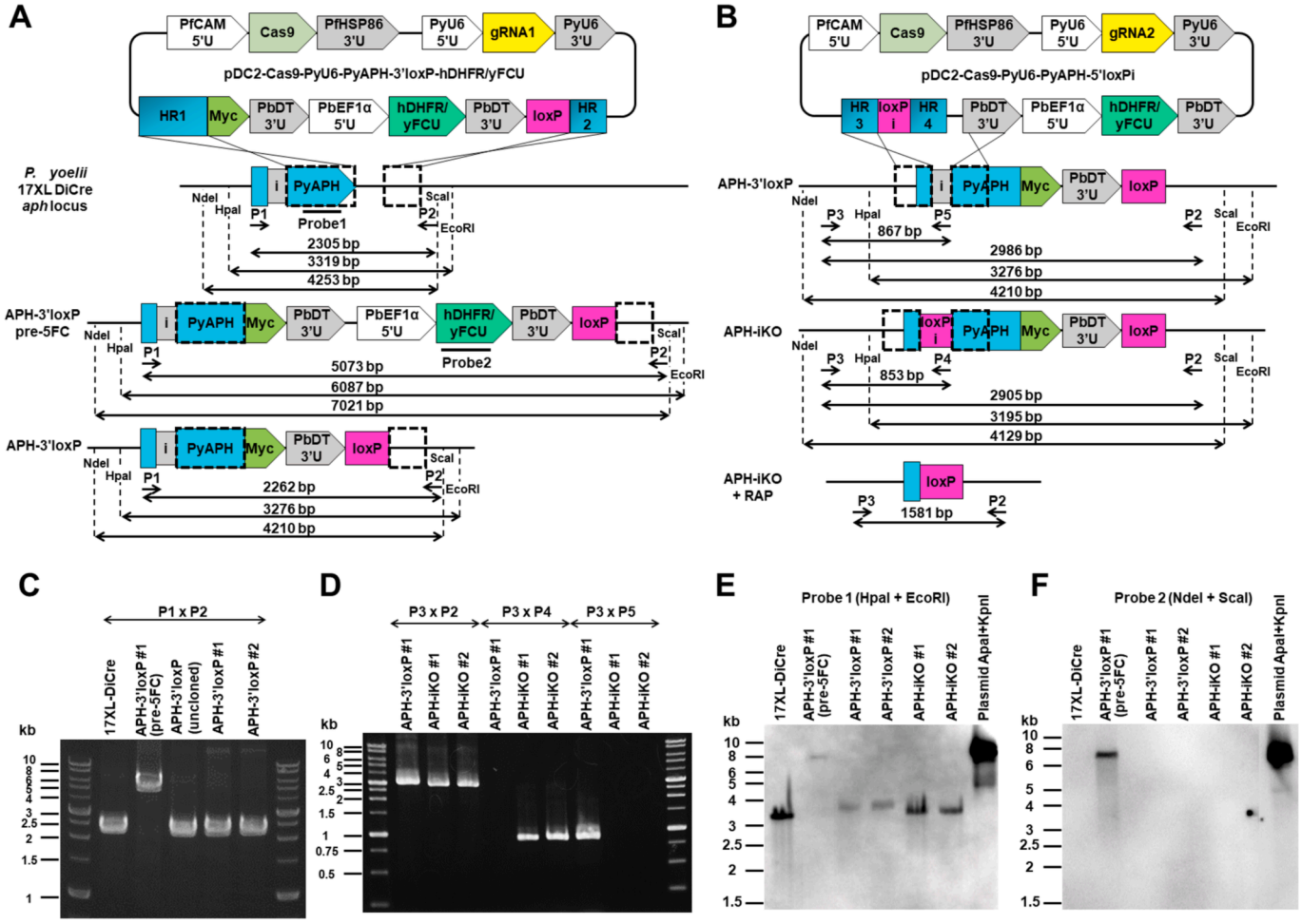

Fig. 1. Generation of PyAPH-iKO parasite lines.
(A) Schematic of the pDC2-Cas9-PyU6-PyAPH-3'loxP-hDHFR/yFCU plasmid and the original (*P. yoelii* 17XL DiCre *aph* locus) and modified *aph* gene locus (APH-3'loxP pre-5FC and APH-3'loxP). (B) Schematic of the pDC2-Cas9-PyU6-PyAPH-5'loxPi plasmid and the modified *aph* gene locus (APH-3'loxP, APH-iKO, and APH-iKO + RAP). 3′U, 3′ untranslated region; 5′U, 5′ untranslated region; CAM, calmodulin; DT, dihydrofolate reductase-thymidylate synthase; EF1α, elongation factor 1 alpha; hDHFR, human dihydrofolate reductase; HR, homologous region; HSP86, heat shock protein 86; i, intron; Pb, *P. berghei*; Pf, *P. falciparum*; Py, *P. yoelii*; U6, U6 small nuclear RNA; yFCU, yeast cytosine deaminase and uridyl phosphoribosyl transferase. Sites cleaved by restriction enzymes, *Hpa*I, *Sca*I, *Nde*I, and *Eco*RI, and sites where oligonucleotide primers and Southern blot probes were designed are shown with the expected sizes by PCR or Southern blot analysis. (C) Genotyping PCR to evaluate the modification of the *aph* gene locus of 17XL DiCre parasite and APH-3'loxP parasites before and after 5FC treatment. For the PyAPH-3'loxP parasite, only clone #1 is shown. (D) Genotyping PCR to evaluate the modification of the *aph* gene locus of APH-3'loxP and APH-iKO parasites before and after RAP treatment. (E) Southern blot analysis for DNA fragments digested with HpaI and EcoRI and detected with probe 1. (F) Southern blot analysis for DNA fragments digested with NdeI and ScaI and detected with probe 2. The pDC2-Cas9-PyU6-PyAPH-5'loxPi plasmid digested with *Apa*I and *Kpn*I was used as a positive control.

2.5. Indirect immunofluorescence assay (IFA)

Blood smears were fixed with 4% paraformaldehyde and 0.075% glutaraldehyde (PFA-GA) in phosphate-buffered saline (PBS) at room temperature (RT) for 15 min. Smears were incubated with 0.1% Triton X-100 in PBS at RT for 10 min for permeabilization, washed twice with PBS at RT for 5 min, and further incubated with 3% BSA in PBS at RT for 1 h for blocking. Subsequently, smears were incubated with primary antibodies at RT for 1 h then further incubated with secondary antibodies with 4′, 6-diamidino-2-phenylindole (DAPI; Invitrogen) at RT for 30 min. Primary antibodies were rabbit anti-Myc monoclonal antibody (1:500; 71D10; Cell Signaling Technology, Danvers, MA, USA), mouse anti-Myc monoclonal antibody (1:500; 9B11; Cell Signaling Technology), mouse anti-Ty monoclonal antibody (1:500; Diagenode, Liege, Belgium), rabbit anti-PyAMA1 (1:250) [27], rabbit anti-PyEBL (1:250) [28], rabbit anti-PyRON5 antibody (1:250) [27], mouse anti-Py235 antibody (1:250; mAb25.86; a kind gift from A. Holder) [29], or mouse anti-PbHSP70 monoclonal antibody (1:20; a kind gift from J. Sattabongkot). Secondary antibodies were Alexa fluor 488-conjugated goat anti-mouse IgG, Alexa fluor 488-conjugated goat anti-rabbit IgG, Alexa fluor 594-conjugated goat anti-rabbit IgG, or Alexa fluor 594-conjugated goat anti-mouse IgG. IFA smears were washed with PBS, briefly air-dried, and mounted with VECTASHIELD antifade medium (Vector laboratories, Burlingame, CA, USA). Images were acquired with a confocal microscope (Nikon A1R; Nikon, Japan). Pearson's correlation coefficient was calculated by imageJ (v1.53) and JaCoP plugin (v2.1.4).

2.6. Rapamycin (RAP) treatment, parasite asexual growth assay, and quantitative PCR

RAP (Sigma-Aldrich) was dissolved with dimethyl sulfoxide (DMSO) at 4 mg/mL and stored at −20 °C [30]. RAP (4 mg/kg) or an equivalent volume of DMSO were intraperitoneally (i.p.) injected into mice infected with PyAPH-iKO parasites when the parasitemias reached 20–30%, and parasites were collected 24 h later. Schizonts were enriched by density gradients using Nycodenz (1.077 g/mL) and incubated *in vitro* at 15 °C for 3 h for maturation. Matured schizonts (10^7) were then intravenously (i.v.) injected to BALB/c mice and RAP (4 mg/kg) or DMSO were immediately administrated (i.p.). Blood was collected at 3, 12, 24, 36, 60, and 84 h after parasite inoculation and thin blood smears and gDNA were prepared. Blood smears were stained with Giemsa's solution and parasitemias were determined.

gDNA samples were used to evaluate the excision efficiency of the *aph* gene locus by RAP-induced DiCre in the generated parasites using quantitative PCR (qPCR) with Power SYBR® Green PCR Master Mix (Thermo Fisher Scientific) and specific primer sets; P14 and P15 for the unique sequence in PyAPH-iKO parasite and P16 and P17 for the *ama1* gene locus (Table S1) using 7500 Real-Time PCR system (Applied Biosystems, Foster City, CA). The excision efficiency of the *pypkac* gene locus by RAP was evaluated as a control [23]. Values for *aph* were normalized to those for *ama1*.

To evaluate the effect on parasite egress and erythrocyte invasion, the percentage of newly invaded ring stage-infected erythrocytes and remaining schizont-infected erythrocytes were examined using blood smears obtained at 3 h after inoculation. Two-way ANOVA and a post-hoc Tukey's multiple comparison test were performed using GraphPad Prism 9 (GraphPad software Inc., San Diego, CA). *P* values less than 0.05 was considered statistically significant.

2.7. Western blotting

Parasite-infected blood samples were treated with 0.1% saponin to lyse the erythrocytes and proteins were extracted with 1% Triton X-100 in PBS containing a protease inhibitor cocktail (cOmplete™: Sigma-Aldrich), separated by SDS-PAGE, then transferred to PVDF membranes. Membranes were immunostained with mouse anti-Myc monoclonal antibody (1:1000), mouse anti-Ty monoclonal antibody (1:250), or mouse anti-PbHSP70 monoclonal antibody (1:200) at RT for 1 h, followed by incubation with HRP-conjugated anti-mouse IgG or anti-rabbit IgG (1:10000; Promega) at RT for 1 h. Bands were visualized using Immobilon Western Chemiluminescent HRP substrate (Millipore) and images were taken by a multipurpose charge-coupled-device (CCD) camera system (LAS-4000 mini) with Multi Gauge software. The band intensities were measured using ImageJ software (v1.53).

2.8. Antisera production

Anti-PyMTRAP (PY17X_0513900) was produced by immunization of a rabbit with a synthetic peptide DGKGKNNQGSGKD (amino acid positions 150–162) which was custom synthesized by Cosmo Bio Co. Ltd. (Tokyo, Japan). The antiserum was affinity-purified using cellulose beads (Cellufine Formyl; JNC corporation, Japan) using the synthetic peptide with the same amino acid sequence custom synthesized by GenScript (Tokyo, Japan). Briefly, after washing cellulose beads in the column, 10 mg of peptide was mixed with 1 mL of beads in 1 mL of coupling buffer (50 mM Na_2CO_3-$NaHCO_3$, pH 8.5) at 4 °C on a rotating shaker. After adding 10 mg of trimethylamine borane (Tokyo Chemical Industry Co. Ltd., Tokyo, Japan), the beads were further shaken at 4 °C for 8–12 h, washed with a blocking buffer (0.2 M Tris–HCl buffer, pH 7.0), and mixed with 10 mg of trimethylamine borane. PyMTRAP peptides on the beads were washed with the elution buffer (0.1 M glycine–HCl, pH 2.5), then with washing buffer (1 M NaCl 1% Triton X-100, pH 7.5), and stored at 4 °C until use. For capturing peptide-specific immunoglobulin from antiserum, 10 mL of rabbit anti-PyMTRAP serum was mixed with the PyMTRAP peptide-conjugated beads at 4 °C for 12 h. After washing, the bound antibodies were eluted with the elution buffer to obtain the purified PyMTRAP antibody.

2.9. Secretion assay

To detect organelle proteins secreted to the merozoite surface, matured schizonts were prepared using Nycodenz and 3 h incubation at 15 °C and were passed through a filter (Φ = 1.2 μm; Sartorius Stedim Biotech, Germany) to obtain free erythrocyte-invasive merozoites, which were maintained at 15 °C throughout the procedure. Merozoites were fixed with PFA-GA for 15 min either immediately or after 10 min incubation at 37 °C, washed with PBS, transferred to the poly-L-lysine coated cover slips, and incubated at RT for 30 min. Merozoites were permeabilized with 0.1% Triton X-100 in PBS for 10 min at RT if required. Merozoites on the cover glasses were then incubated with 3% BSA in PBS at RT for 1 h for blocking, incubated with primary antibodies at RT for 1 h, washed with PBS, and incubated with secondary antibodies at RT for 30 min. To observe protein secretion by merozoites attached to erythrocytes, filtered merozoites were incubated with fresh erythrocytes at 37 °C for 10 min, then fixed with PFA-GA for 15 min. For some experiments, an actin polymerization inhibitor, cytochalasin D (final concentration of 1 μM; Sigma-Aldrich) or a same volume of its solvent DMSO was added to the matured schizont culture 1 h before filtration, then washed twice using incomplete medium (PyCM without AlbuMax I) before filtration. Primary antibodies were rabbit anti-PyAMA1 (1:250), rabbit anti-MTRAP (1:10), rabbit anti- PyEBL (1:250), and mouse anti-Py235 (1:250). The chicken anti-MSP1 antibody (1:500) [22] was used to identify merozoites and mouse anti-*Plasmodium berghei* HSP70 monoclonal antibody (obtained from J. Sattabongkot, which cross-reacts with HSP70 orthologs of other *Plasmodium* spp.) [31] was used to assure the integrity of the parasite membrane. The Alexa fluor 488-conjugated goat anti-chicken IgY, Alexa fluor 568-conjugated goat anti-mouse IgG, Alexa fluor 647-conjugated anti-rabbit IgG, and Alexa fluor 647-conjugated anti-mouse IgG were used as secondary antibodies (1:500). IFA images were obtained with a confocal microscope (Nikon A1R) under the fixed laser condition. Sum intensity and secretion area (%, pixel numbers positive for the signal of

target proteins per MSP1 signal positive pixel numbers) were analyzed using NIS-elements software (Nikon) and significant differences were examined by Mann-Whitney *U* test.

2.10. Time-lapse imaging

Erythrocyte invasive merozoites were purified from RAP- or DMSO-pretreated matured schizonts as described [22]. Fresh mouse erythrocytes were adjusted to 25,000 erythrocytes/μL with complete culture medium for *P. yoelii* (PyCM, RPMI1640 medium supplemented with 0.23% sodium bicarbonate, 1% AlbuMax I, 25 mM HEPES, 50 μg/mL hypoxanthine, and 10 μg/mL gentamicin), and kept at 37 °C. The settings for time-lapse imaging were as described [8]. Briefly, the prepared erythrocytes were transferred to μ-Slide VI 0.4 chambers (ibidi, Germany) and kept at RT for 10 min to allow the erythrocytes to settle to the bottom of the chamber. Then, purified merozoites were added and the chambers were placed on the stage of an inverted microscope (Nikon Ti2-E) for video imaging with a CCD camera (ORCA-R2; Hamamatsu Photonics, Japan) for 40 min. Merozoites that attached to erythrocytes were assessed for 5 min to characterize subsequent invasion steps. The two-tailed Fisher's exact test was used for statistical analysis.

3. Results

3.1. Expression of APH in P. yoelii

To evaluate the expression and function of APH in *P. yoelii*, transgenic *P. yoelii* lines were created whose *aph* gene locus could be excised by RAP treatment. Firstly, the 3′ side of the *aph* gene locus of *P. yoelii* 17XL DiCre parasite was independently modified twice to yield two APH-3'loxP parasite clones (Fig. 1A). Two PyAPH-3'loxP clones were further independently modified to yield PyAPH-iKO (Fig. 1B). PCR with primers P1 and P2 amplified a ~ 2.3-kb band from the parental 17XL DiCre parasite, a ~ 5-kb band from PyAPH-3'loxP parasite clone #1 before 5FC treatment, and a ~ 2.3-kb band from PyAPH-3'loxP parasites (uncloned and two clones) after 5FC treatment, confirming the expected modification of the target region after each step (Fig. 1C). Subsequent PCR amplified a ~ 3-kb band from APH-3'loxP clone #1 and a ~ 2.9-kb band from APH-iKO clones with primers P3 and P2; but ~0.9-kb bands were only amplified from APH-iKO clones with primers P3 and P4, and from the APH-3'loxP clone with primers P3 and P5 (Fig. 1D). These are consistent to the sizes expected based upon the transgenic design. Southern blot analysis for DNA fragments digested with *Hpa*I and *Eco*RI and detected with the probe 1 revealed a ~ 3.3-kb band for the parental 17XL DiCre parasite line, a > 6-kb band for PyAPH-3'loxP consistent with the insertion of the hDHFR/yFCU expression cassette, an ~3.4-kb band for PyAPH-3'loxP clones #1 and #2 after 5FC treatment consistent with the removal of the hDHFR/yFCU expression cassette, and an ~3.3-kb band for PyAPH-iKO clones #1 and #2 consistent with the replacement of the intron region (Fig. 1E). Southern blot digested with *Nde*I and *Sca*I and detected with the probe 2 showed an ~7-kb band only for PyAPH-3'loxP before 5FC treatment, indicating the absence of the hDHFR/yFCU expression cassette in the APH-3'loxP and APH-iKO clones (Fig. 1F). The pDC2-Cas9-PyU6-PyAPH-5'loxPi plasmid digested with *Apa*I and *Kpn*I was used as a positive control and was positive for both probes.

In *T. gondii*, conditional knockdown of TgAPH resulted in the loss of MIC2 and AMA1 secretion. Thus, to characterize the *Plasmodium* MIC2 homolog, MTRAP, we generated a transgenic *P. yoelii* line in which the MTRAP C-terminal end was fused with a Ty-tag (Fig. S1A and B). Western blot analysis revealed that the signals detected with anti-Ty antibody and the anti-PyMTRAP antibody generated for this study showed similar sized bands (Fig. S1C and D) as well as completely overlapped IFA signals (Fig. S1F), thus validating that the anti-MTRAP antibody detected native PyMTRAP protein.

To evaluate the *P. yoelii* APH (PyAPH) cellular localization, IFA was performed at the schizont stage (Fig. 2A) using PyAPH-iKO parasites with anti-Myc antibody and known marker proteins including AMA1 (microneme), MTRAP (microneme), EBL (dense granule-like organelle in Py17XL), RON5 (rhoptry neck), Py235 (rhoptry), and HSP70 (cytosol). APH-Myc signals were largely overlapped with MTRAP-Ty signals with the highest Pearson's correlation coefficient value (0.76 ± 0.09), but less overlapped with AMA1 signals (0.60 ± 0.10). IFA of *P. yoelii* schizonts expressing MTRAP-Ty dual-stained with anti-Ty and anti-AMA1 antibodies also showed that these two signals did not have significant overlap (Fig. S1E). This result suggests that PyAPH is only associated with micronemes containing MTRAP, but not AMA1-containing micronemes or only a part of AMA1-containing micronemes associate with APH.

3.2. APH protein expression was reduced to ~11% 24 h after RAP treatment

The effect of RAP administration to PyAPH-iKO parasites on the APH expression level was evaluated using synchronized parasites. Mature schizonts obtained by Nycodenz-enrichment and *in vitro* incubation at 15 °C were inoculated into mice and RAP or DMSO were immediately administrated (i.p.). Western blot analysis revealed that RAP-treated clones expressed a low amount of Myc-tagged APH compared to the

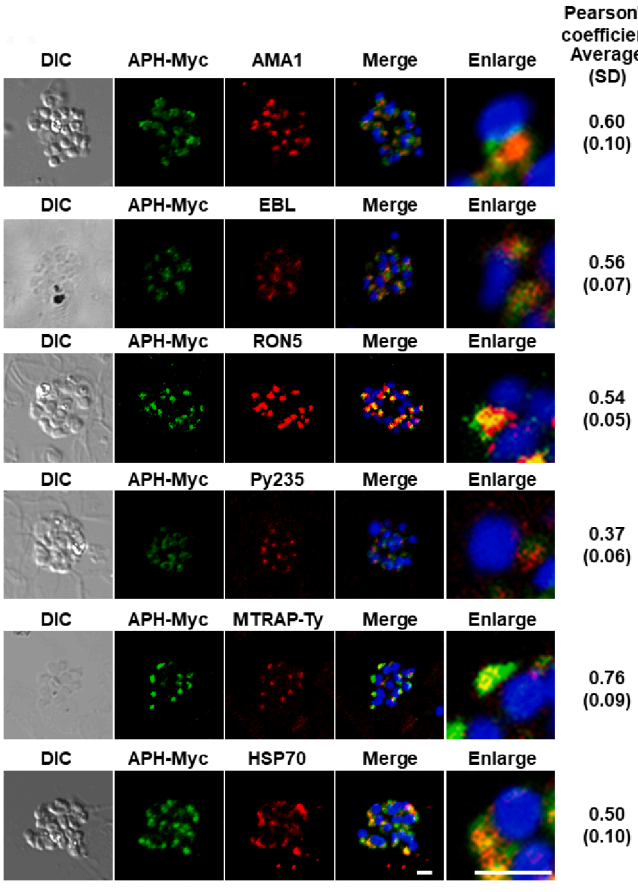

Fig. 2. Indirect immunofluorescence assay for *P. yoelii* APH.
IFA images of the schizont stage of PyAPH-iKO parasites. Fluorescent signals with anti-Myc antibody (green, PyAPH) were merged with DAPI nucleus signals (blue), and marker protein signals (red: AMA1, microneme; EBL, dense granule-like organelle; RON5, rhoptry neck; Py235, rhoptry; MTRAP-ty, microneme; and HSP70, cytoplasm). Differential interference contrast (DIC) images are also shown. Scale bars, 2 μm. Average and standard deviation (SD) of the Pearson's correlation coefficient values were from 10 images. (For interpretation of the references to colour in this figure legend, the reader is referred to the web version of this article.)

DMSO-treated controls 24 h later (Fig. 3A and S2A arrow). When the APH band intensities were normalized by the intensities of HSP70 bands, the amounts of APH in RAP-treated clones were 12% and 11% for clones #1 and #2, respectively, compared to the DMSO-treated controls (Fig. 3B and S2B). An extra band at ~21 kDa was detected in the DMSO-treated parasites with anti-Myc antibody which was not seen in the parasites before DMSO administration (Fig. 3A and S2A arrowhead). This ~21-kDa band was repeatedly detected from the independently prepared parasite samples, suggesting that PyAPH expressed in PyAPH-iKO parasite was somehow processed by DMSO administration. Nonetheless, these data indicated that APH was dramatically reduced in PyAPH-iKO parasites by RAP administration and validated the usage of these parasite clones for functional analysis.

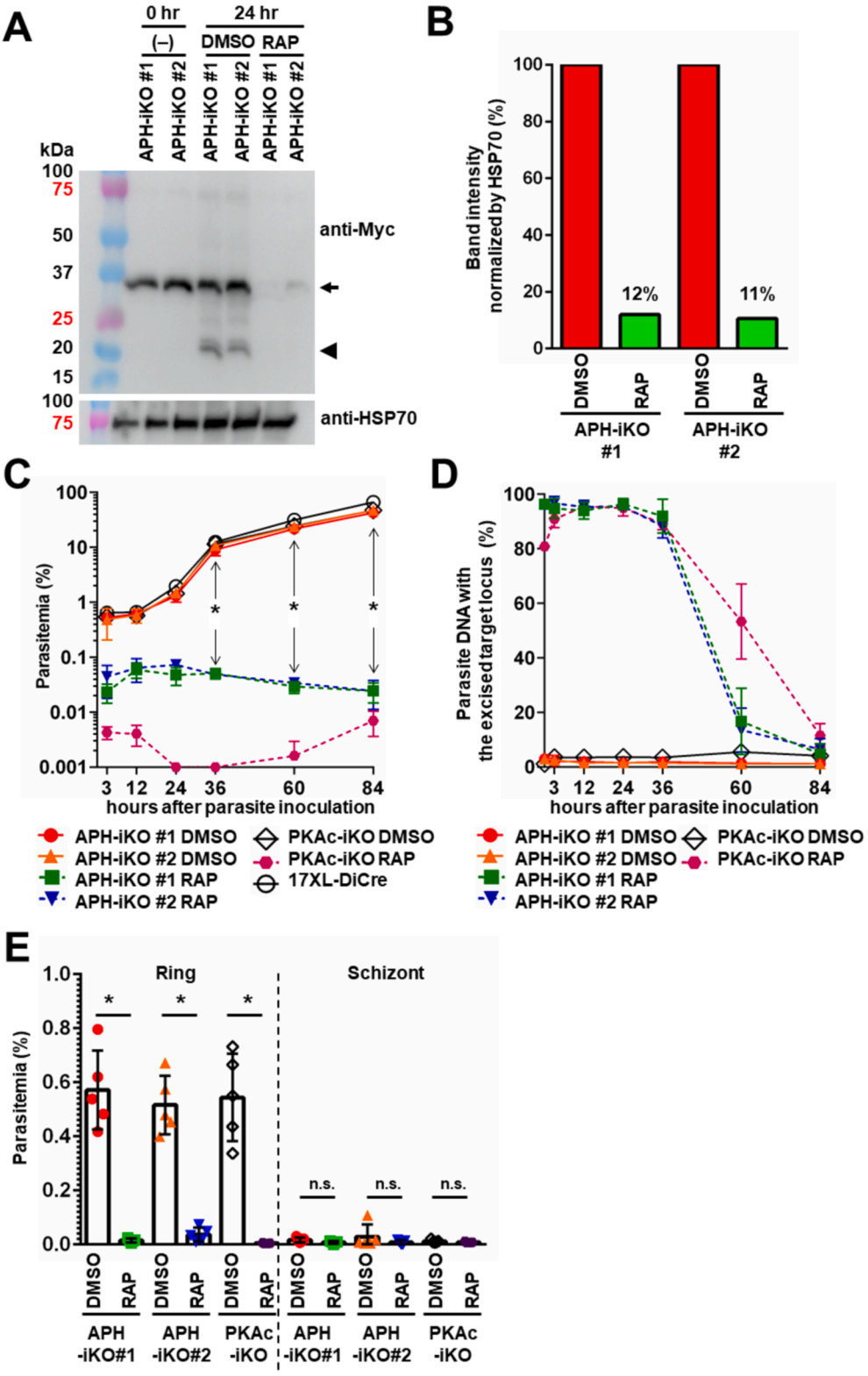

Fig. 3. APH expression, *in vivo* asexual growth, and erythrocyte invasion by RAP-treated PyAPH-iKO blood stage parasites. (A) Top, Western blot for Myc-tagged PyAPH with anti-Myc antibody. Bands matching the theoretical molecular weight of Py APH-Myc (~32 kDa) are indicated with an arrow. Extra bands at ~21 kDa are indicated with an arrowhead. Bottom, *P. yoelii* HSP70 bands are detected and used as loading controls. (B) The intensities of the bands on the Western blots were quantified and the values of ~32-kDa PyAPH bands were normalized by those of HSP70 bands. Obtained values of DMSO-treated control parasites were set to 100%. (C) Parasitemias in mice were monitored for PyAPH-iKO clones #1 and #2, and a PyPKAc-iKO clone (n = 5 for each) at 3, 12, 24, 36, 60, and 84 h after inoculation of matured schizonts pre-treated with RAP- or DMSO followed by immediate administration of RAP or DMSO, respectively. Parasitemias of the Py17XL-DiCre parasites were also monitored as controls without drug administration. Asterisks indicate that the parasitemias of RAP-treated PyAPH-iKO clones were significantly lower than those of DMSO-treated PyAPH-iKO groups ($p < 0.0001$) by the post-hoc Tukey's multiple comparison test following two-way ANOVA. (D) Relative values of the parasite DNA with the excised *aph* or *pkac* gene locus to all parasite DNA obtained from samples are shown in panel C. (E) Results of the assessment of *in vivo* egress and erythrocyte invasion for PyAPH-iKO clones #1 and #2, and a PyPKAc-iKO clone (n = 5 for each). Asterisks indicate significant differences ($p < 0.0001$).

3.3. Deletion of APH severely affected the P. yoelii asexual growth and erythrocyte invasion, but was not lethal

Next, the effect of the excision of the *aph* gene locus on parasite asexual growth was examined. PyAPH-iKO clones treated with RAP or DMSO for 24 h were synchronized, and mature schizonts were injected into fresh BALB/c mice with RAP or DMSO, then parasitemias were monitored for 84 h without additional RAP or DMSO administration. In addition to a parental 17XL-DiCre parasite, a PKAc-iKO parasite clone, in which the *pkac* gene locus coding for an essential protein for the erythrocyte invasion can be excised with RAP, was also monitored as a control. With DMSO, two APH-iKO clones and the PKAc-iKO clone showed parasitemias of >0.5% at 3 h and grew similar to the parental DiCre parasite (Fig. 3C). When RAP was administered, the parasitemias of theAPH-iKO clones #1 and #2 were 0.02 ± 0.01% and 0.04 ± 0.03%, respectively, much lower than the parasitemia of the control DMSO-treated groups, but higher than that of the PKAc-iKO clone (0.004 ± 0.001%), suggesting that APH-iKO had important, but not essential roles during egress or the cell invasion process. At 12 h, the parasitemias of RAP-treated APH-iKO clones and the PKAc-clone were not reduced, suggesting non-essential roles of these proteins during intraerythrocytic growth up to this time point. At 24 h when synchronized parasites were matured and were invading new erythrocytes, the parasitemia of the RAP-treated PKAc-iKO clone was further reduced to 0.001 ± 0.000%, whereas the parasitemias of RAP-treated APH-iKO clones #1 and #2 were not reduced (0.05 ± 0.02% and 0.07 ± 0.01%, respectively), but also not increased like for the DMSO-treated groups; again suggesting roles, albeit non-essential, of APH during egress or cell invasion.

To exclude a potential low excision efficacy of the *aph* gene locus in APH-iKO clones during this experiment, a proportion of the parasites in which the target gene locus was excised were monitored (Fig. 3D). We found that the *aph* gene locus was excised in ~95% of the RAP-treated parasites from 0 to 36 h. Together these data indicate that even though the *aph* gene locus was not intact past 24 h, some parasites were able to egress and invade new erythrocytes.

At 36 h, the parasitemia of the RAP-treated PKAc-iKO clone was not reduced further and increased at 60 and 84 h, which is consistent to the increased proportion of the parasites in which the target gene locus was intact; suggesting that the RAP concentration in the mouse blood became too low to excise the target gene locus.

To further evaluate the roles of APH in *P. yoelii* on egress and cell invasion, schizont-infected erythrocytes and erythrocytes with newly invaded ring stage parasites were separately counted from the smears prepared 3 h after inoculation. The effects on the PKAc-iKO parasites were consistent to a report showing that the ring stage parasitemia of the RAP-treated group (0.004 ± 0.001%) was significantly lower than that of the DMSO-treated group (0.54 ± 0.16%, $p < 0.0001$) and no difference was detected for the schizontemias between the two groups (Fig. 3E) [23], validating that this assay was properly conducted. The ring stage parasitemias of the RAP-treated PyAPH-iKO clones #1 and #2 were 0.02 ± 0.01% and 0.04 ± 0.03%, respectively, significantly lower than those of DMSO-treated groups (0.57 ± 0.15% and 0.52 ± 0.11%, respectively) (Fig. 3E). The schizontemias of the RAP-treated PyAPH-iKO clones #1 and #2 were 0.01 ± 0.00% and 0.01 ± 0.01%, respectively, not significantly different from those of the DMSO-treated groups (0.02 ± 0.01% and 0.03 ± 0.04%, respectively) (Fig. 3E); suggesting that APH plays a role during erythrocyte invasion but is not observably involved in the egress process of *P. yoelii*.

3.4. APH is required for secretion of MTRAP and AMA1, but not EBL and Py235

To compare with the observations for *T. gondii*, in which MIC2 and AMA1 secretion was inhibited when TgAPH was knocked down, we examined the consequence of *aph* gene locus excision in *P. yoelii* on the secretion of invasion-related molecules; namely, MTRAP (MIC2 homolog), AMA1, EBL, and Py235. By IFA, we found trace or absent signals of MTRAP and AMA1 on the surface of PyAPH-iKO merozoites prepared from RAP-treated matured schizonts even after 10 min incubation at 37 °C, whereas both signals were clearly visible on merozoites treated with DMSO (Fig. 4A and C). HSP70 was detected from the Triton X-100-treated merozoites, but not from the untreated merozoites, indicating that the plasma membranes of the test samples were intact. Quantitative assessment revealed that both the sum intensities and signal positive areas for AMA1 and MTRAP on the merozoite surface were significantly lower than those of DMSO-treated parasites at 0 min and after 10 min incubation (Fig. 4B and D, $p < 0.0001$). In contrast to AMA1 and MTRAP, no obvious differences were observed for the secretion of EBL and Py235 between RAP- and DMSO-treated merozoites, indicating that the excision of the *aph* gene locus had no effect on the secretion of these proteins (Fig. 4E–H).

3.5. Deletion of APH impaired P. yoelii internalization into erythrocytes, but had no effect on tight junction formation

Time-lapse image analysis was performed to describe the invasion steps affected by the absence of APH in *P. yoelii*. Merozoites pretreated with RAP or DMSO were incubated with fresh erythrocytes and approximately 50–70 merozoites that attached to the erythrocytes were evaluated for 5 min for (i) erythrocyte deformation, (ii) detachment from the erythrocyte, (iii) parasite internalization into the erythrocyte, and (iv) echinocytosis. Examples are presented for successful invasion by the DMSO-treated merozoite (Fig. 5A and video 1) and unsuccessful invasion by the RAP-treated merozoite (Fig. 5A and video 2). We found no significant difference for the proportion of merozoites that were able to deform erythrocytes between RAP-treated (84% and 79% for clones #1 and #2) and DMSO-treated parasites (88% and 74%, respectively) (Fig. 5B). Erythrocyte deformation is linked to merozoite gliding motility [5], and is likely mediated by TRAP family proteins. Thus, this result was unexpected because the secretion of MTRAP, a TRAP family member expressed at the merozoite stage, was severely impaired in RAP-treated APH-iKO parasites.

We observed that 60% (25/42) and 43% (21/36) of DMSO-treated PyAPH-iKO clones #1 and #2 merozoites that deformed erythrocytes showed echinocytosis, whereas the ratios of RAP-treated merozoites were significantly lower at 8% (4/52) and 7% (3/41), respectively (Fig. 5C, $p < 0.0001$). These data indicated that the excision of the *aph* gene locus had a strong impact on merozoite internalization into the erythrocyte and the subsequent echinocytosis event, but still 7– 8% were able to complete the invasion process, consistent with the observation that RAP-treated parasites were able to slowly proliferate (Fig. 3C). The ratio of the merozoites not detached from the erythrocyte per those attached but not internalized to the erythrocyte were 81% (39/48) and 82% (31/38) for RAP-treated APH-iKO clones #1 and #2 merozoites, significantly higher than the 53% (9/17) and 40% (6/15) observed for DMSO-treated merozoites, respectively (Fig. 5D, $p < 0.05$). This observation that un-internalized merozoites were kept attached to the erythrocyte membrane, indicated that the tight junction was established between the merozoite and the erythrocyte even following APH deletion.

3.6. MTRAP is APH-independently secreted to the surface of merozoites that attached to the erythrocyte

To explore the possible reasons why APH-deficient merozoites were able to deform erythrocyte membranes, we firstly reconfirmed whether the observed erythrocyte deformation by *P. yoelii* was linked to actomyosin motor activity. We performed time-lapse image analysis during the erythrocyte invasion using a wild type 17XL parasite line treated with cytochalasin D (CytD), an actin polymerization inhibitor, to inhibit the merozoite motor activities (Fig. 6A and video 2) or control DMSO (Fig. 6A and video 1). After attaching to erythrocytes, erythrocyte

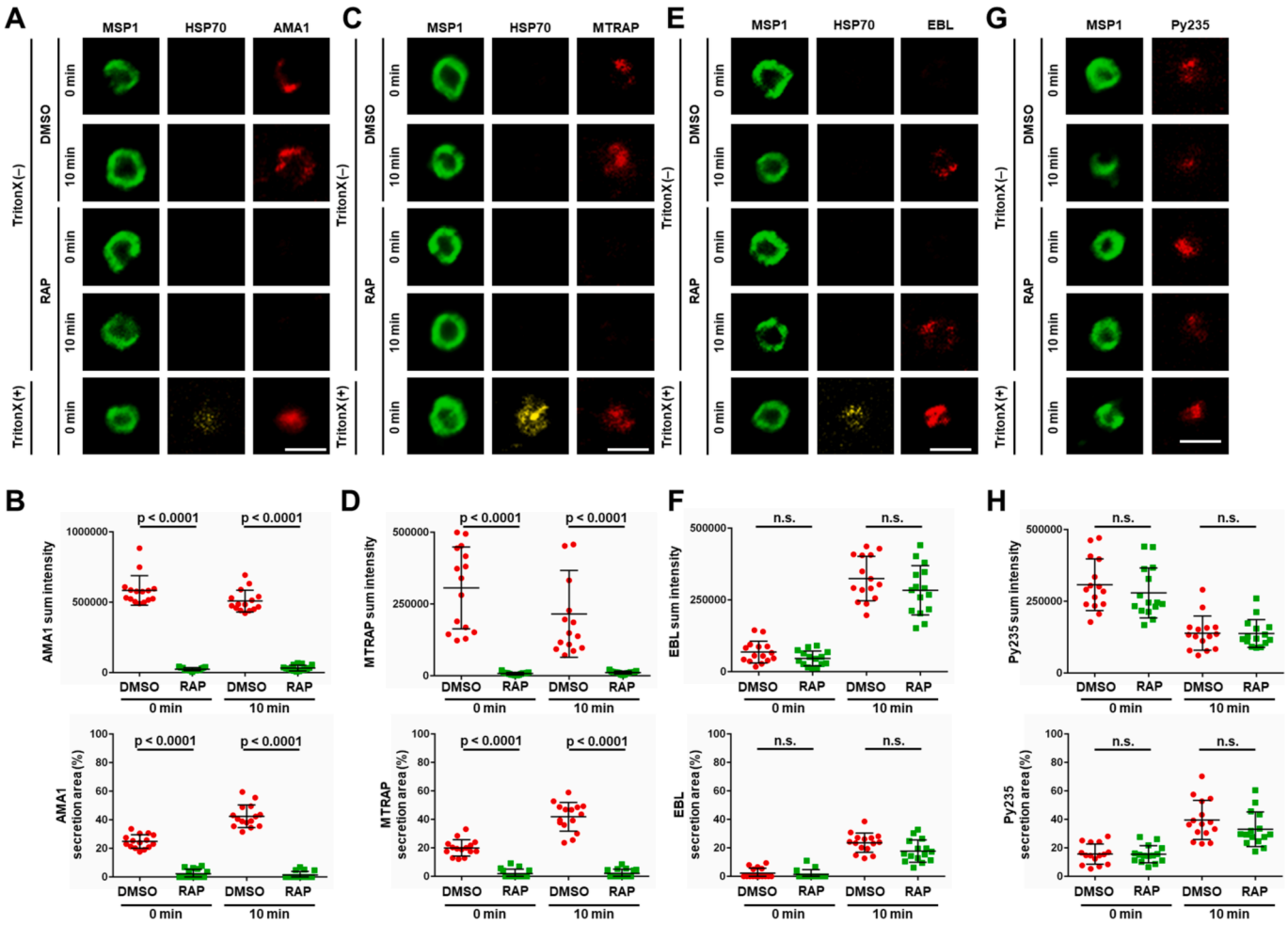

Fig. 4. Protein secretion by RAP-treated PyAPH-iKO merozoites.
Purified invasive merozoites of the PyAPH-iKO parasite pretreated with RAP or DMSO were labeled with a panel of antibodies against AMA1 (A), MTRAP (C), EBL (E), or Py235 (G) at 0 and 10 min after incubation at 37 °C with or without permeabilization with Triton X-100 (TritonX (+) or (−)). Target proteins AMA1, MTRAP, EBL, and Py235 are colored in red. MSP1 (green) and HSP70 (yellow) were counterstained. Scale bar, 2 μm. Sum intensity (top) and secretion area (bottom) of signals for AMA1 (B), MTRAP (D), EBL (F), or Py235 (G) of 15 merozoites were obtained by NIS-elements software and significant difference was examined by Mann-Whitney *U* test. (For interpretation of the references to colour in this figure legend, the reader is referred to the web version of this article.)

deformation events by CytD-treated merozoites (Fig. 6B; 9% (3/35)) were significantly lower than those by DMSO-treated merozoites (Fig. 6B; 68% (26/38)) and none of the CytD-treated merozoites were able to complete the invasion process. These data confirmed that merozoite actomyosin motor activities were indeed linked to the erythrocyte deformation by *P. yoelii* merozoites.

Secondly, we examined whether micronemes could discharge when merozoites were attached to the erythrocyte, and thereby are able to start to glide and deform erythrocytes. RAP- or DMSO-treated merozoites were incubated with fresh mouse erythrocytes at 37 °C for 10 min, then labeled with anti-AMA1 or anti-MTRAP antibodies. Because DMSO-treated merozoites are quickly internalized, the chance to capture merozoite images attached on the erythrocyte was low. Thus, we decided to assess microneme secretion in the presence of CytD. Under both the absence or presence of CytD, MTRAP, but not AMA1, was detectable on the surface of RAP-treated merozoites (Fig. 7A and C). Quantitative assessment revealed that both the sum intensity and signal positive areas for AMA1 on the RAP-treated merozoites were significantly lower than those of DMSO-treated parasites (Fig. 7B, $p < 0.001$). Although the sum intensities of MTRAP signals on the RAP-treated merozoites were significantly lower than those of DMSO-treated merozoites ($p < 0.001$), no differences were detected on the signal positive areas between RAP- and DMSO-treated merozoites (Fig. 7D); indicating that lower amounts of MTRAP, but not AMA1, were secreted and distributed on the surface of merozoites that attached to erythrocytes. Because protein secretion was evaluated 10 min after merozoite incubation at 37 °C for both free merozoites (Fig. 4) and merozoites with erythrocytes (Fig. 7), we interpreted that the contact of merozoites to the erythrocytes induced the secretion of MTRAP.

4. Discussion

In this study we examined the function of *P. yoelii* APH (PY17X_0716800), whose ortholog in *T. gondii* has a role in parasite egress and cell invasion and is essential for survival [20]. Unlike *T. gondii*, we found that *P. yoelii* APH is primarily required for erythrocyte invasion, but not for egress during the blood stage. Egress of *T. gondii* is dependent on the disruption of the parasitophorous vacuole membrane by a microneme protein, *Toxoplasma* perforin-like protein 1 (TgPLP1) [32]; thus it is reasonable that knockdown of TgAPH reduced the egress of this parasite. In contrast, egress of malaria parasites is initiated by the secretion of the subtilisin-like serine protease PfSUB1 from exonemes, an organelle distinct from micronemes [21]. Thus, our observation that loss of APH does not impact parasite egress can be explained by no involvement of APH in exoneme discharge in malaria parasites.

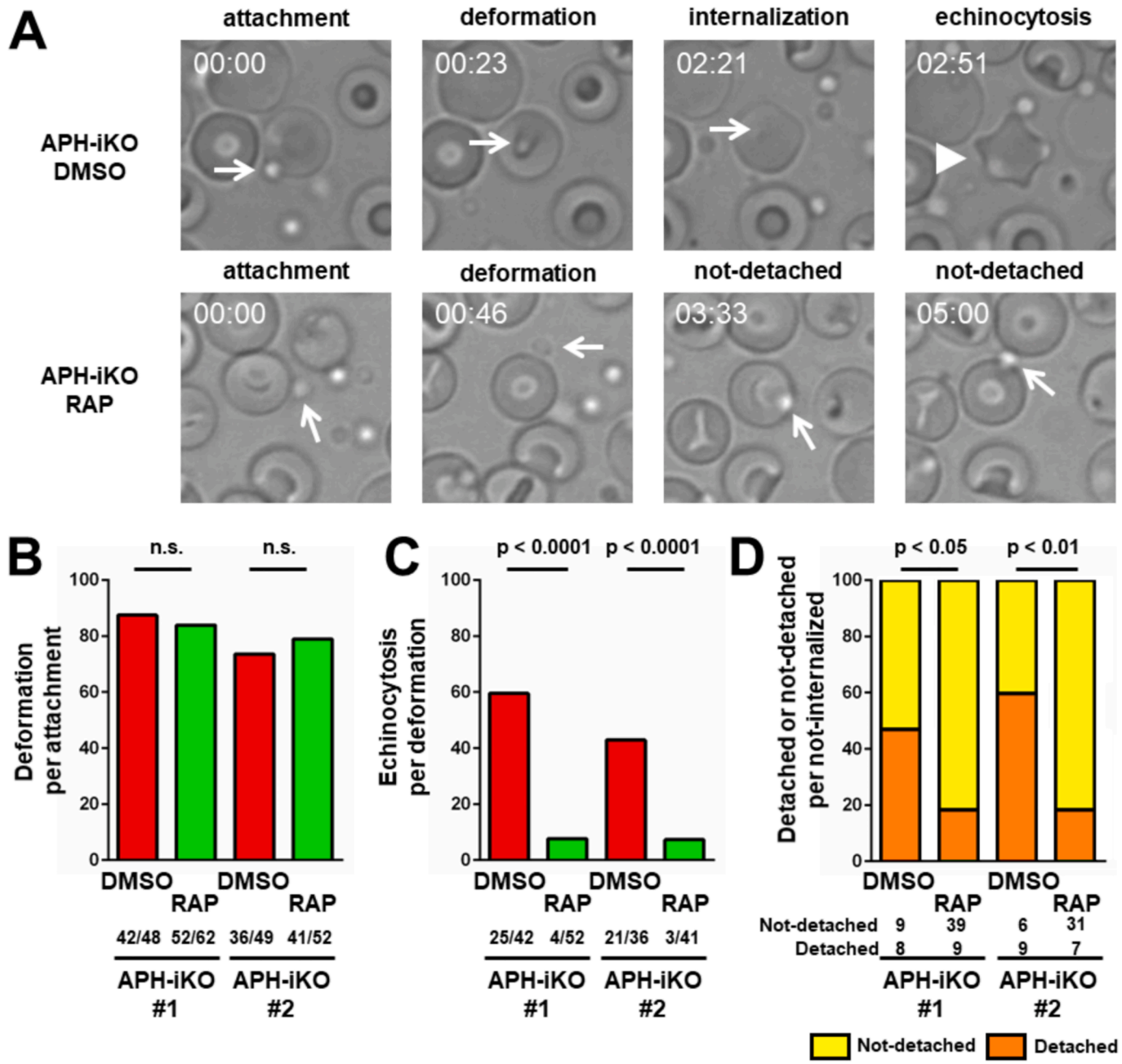

Fig. 5. Time-lapse image analysis of RAP-treated PyAPH-iKO parasites during erythrocyte invasion.
(A) Images of different steps during erythrocyte invasion (initial attachment, erythrocyte deformation, internalization, and echinocytosis) by DMSO- or RAP-treated PyAPH-iKO parasites captured from representative time-lapse videos (Videos 1 and 2, respectively). For the RAP-treated PyAPH-iKO parasite (clone #1), a merozoite is shown that was not internalized yet not detached from the erythrocyte 5 min after the initial attachment. Arrows and an arrowhead indicate merozoites and an erythrocyte exhibiting echinocytosis, respectively. (B) Percentage of the deformation event per the initial attachment event. (C) Percentage of the echinocytosis event per the deformation event. (D) Percentage of the merozoites detached or not detached from the erythrocyte per the merozoites not internalized into the erythrocyte. The observed numbers of each event are shown below each graph. Significant difference was examined by two-tailed Fisher's exact test. n.s. indicates not significant ($p \geq 0.05$).

This study demonstrated that IFA signals of APH in *P. yoelii* merozoites were highly overlapped with PyMTRAP signals, but less overlapped with PyAMA1 signals. Nevertheless, secretion of both PyMTRAP and PyAMA1 were impaired by the excision of the *aph* gene locus. These suggest that interaction of PyAPH and PA is directly responsible for PyMTRAP secretion, but the secretion of PyAMA1 may be indirectly triggered. This is consistent to the observation of erythrocyte contact-dependent secretion of PyMTRAP, but not PyAMA1 (Fig. 7). However, it is unclear if secretion of the TRAP family protein is prerequisite of AMA1 secretion or not, which needs future investigation. In addition, we emphasize that our observation that deletion of APH in *P. yoelii* had a significant impact on the secretion of PyMTRAP and PyAMA1, but not EBL secretion; which complements a report by Ebrahimzadeh et al. (2019), who showed that the disruption of another pleckstrin homology domain-containing protein PH2 in *P. falciparum* affected EBL secretion, but not PfAMA1 secretion. Thus, two different pleckstrin homology domain-containing proteins, PfAPH and PfPH2, appear to regulate exocytosis of different sets of microneme vesicles in a mutually exclusive manner.

Our unexpected finding that *P. yoelii* without APH was able to deform

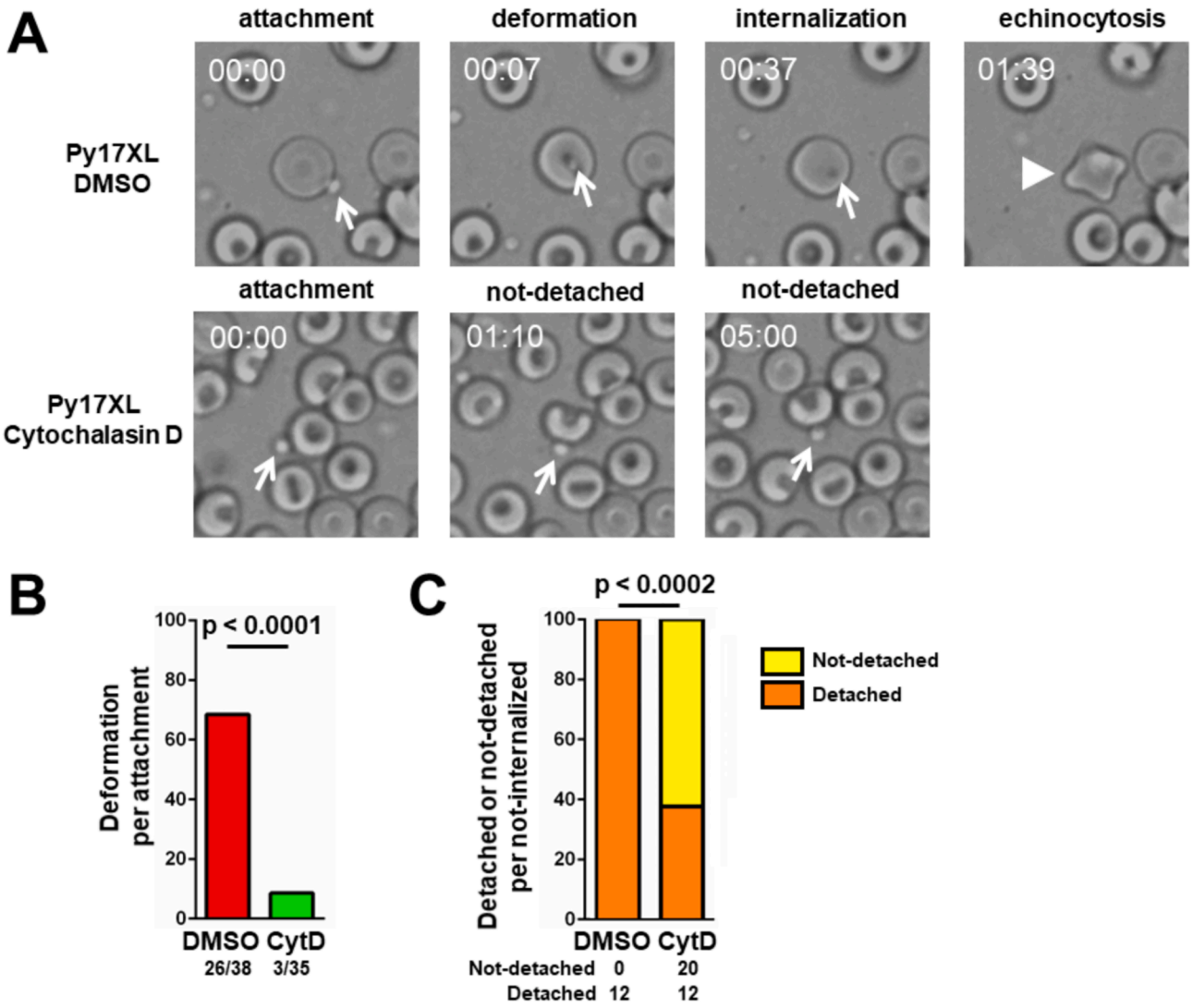

Fig. 6. Time-lapse image analysis of cytochalasin D-treated wild type 17XL parasites during erythrocyte invasion.
(A) Images of different steps during the erythrocyte invasion (initial attachment, erythrocyte deformation, internalization, and echinocytosis) of DMSO- or cytochalasin D (CytD)-treated 17XL wild type parasites captured from representative time-lapse videos (Videos 3 and 4, respectively). For the CytD-treated parasite, a merozoite is shown that was not internalized yet not detached from the erythrocyte 5 min after the initial attachment. Arrows and an arrowhead indicate merozoites and an erythrocyte exhibiting echinocytosis, respectively. (B) Percentage of the deformation event per the initial attachment event. (C) Percentage of the merozoites detached or not detached from the erythrocyte per the merozoites not internalized into the erythrocyte. The observed numbers of each event are shown below the graphs. Significant difference was examined by two-tailed Fisher's exact test.

erythrocytes may be explained by the erythrocyte contact-dependent secretion of PyMTRAP; however, the involvement of PyMTRAP in merozoite gliding motility is not yet determined. Because MTRAP orthologs are dispensable in *P. falciparum* and *P. berghei* during asexual blood stage development [33], other proteins may be responsible for erythrocyte deformation, such as another TRAP member and merozoite microneme protein, *Plasmodium* thrombospondin-related apical merozoite protein (PTRAMP) [34].

Although we did not detect PyAMA1 secretion from the RAP-treated APH-iKO clone even after the merozoite contact with erythrocytes, 7–8% of merozoites were able to invade. Two possibilities may be raised; one is that some merozoites utilize a low amount of PyAMA1 that could be secreted after PyMTRAP secretion, and the other is that some merozoites may be able to invade without PyAMA1. The latter case is supported by *piggyBac* transposon insertional mutagenesis analysis of *P. falciparum*; which revealed that the mutagenesis index score (MIS) of PfAMA1 was 0.78 (on a scale of 0–1, when a lower MIS indicates a lower possibility of essentiality), suggesting that some merozoites were able to invade without PfAMA1 [35,36]. Relatively stable parasitemia of the RAP-treated PyAPH-iKO clones compared to the rapid reduction of parasitemia of the RAP-treated PyPKA-iKO clone from 3 to 24 h (Fig. 3C) are consistent to the results of this mutagenesis analysis; specifically, the MIS of PfAPH was 0.68 and that of PfPKAc was 0.2.

In conclusion, we generated transgenic parasite lines for which PyAPH can be conditionally knocked out using the DiCre conditional recombinase system. We demonstrated that PyAPH has an important role for the secretion of PyMTRAP and PyAMA1, thus excision of the *aph* gene locus severely impaired erythrocyte invasion and parasite asexual growth. We showed that PyAPH colocalized with PyMTRAP, but not with PyAMA1 and proposed that different direct signals exist to trigger the secretion of PyMTRAP *versus* PyAMA1. We also proposed that erythrocyte-contact may trigger PyMTRAP secretion. Further investigation of these new findings will provide a better understanding of the molecular mechanism of erythrocyte invasion by malaria parasites and may lead to the discovery of novel drug targets.

Supplementary data to this article can be found online at https://doi.

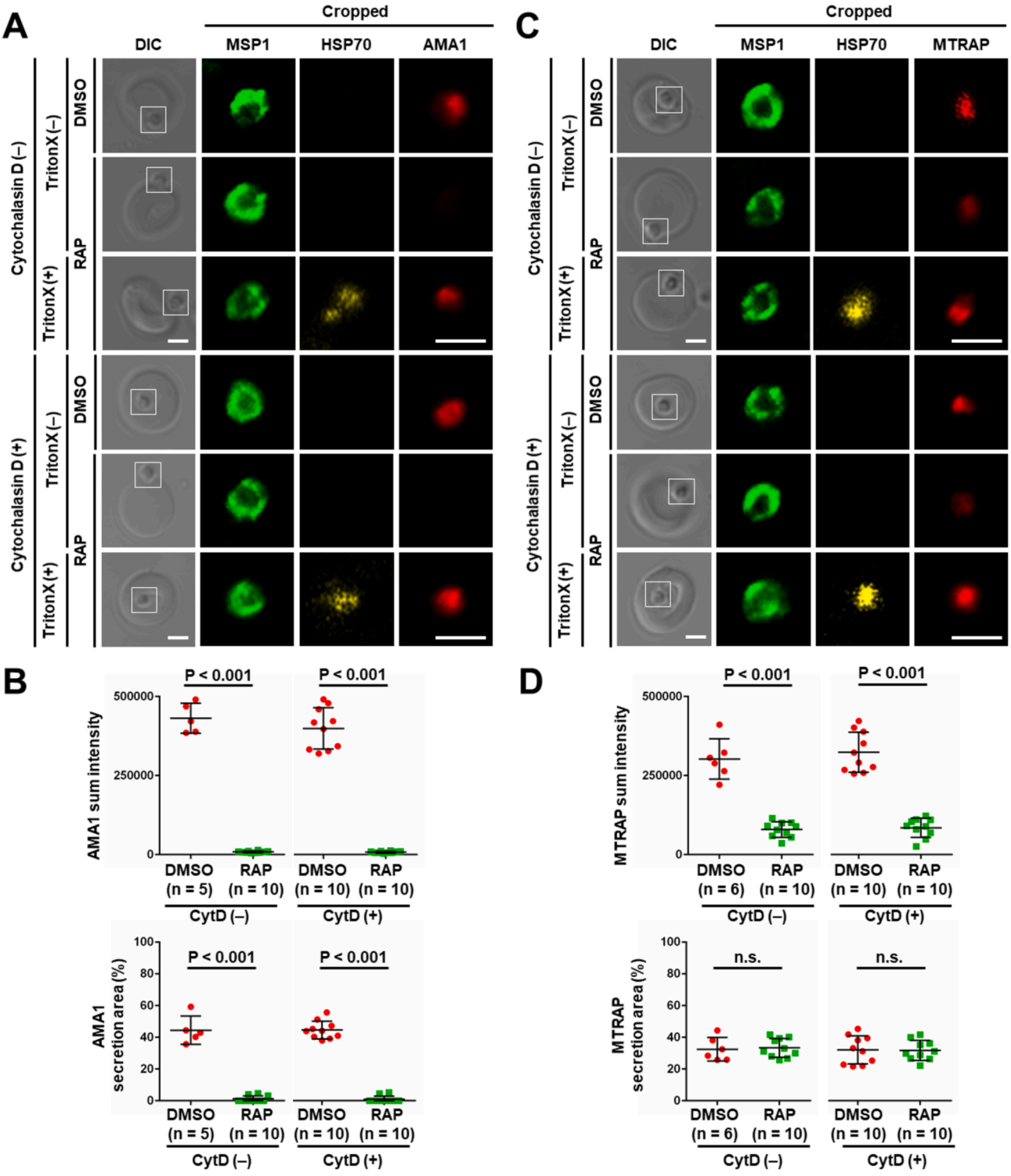

Fig. 7. Protein secretion by RAP-treated PyAPH-iKO merozoites that attached to the erythrocytes.
Purified invasive merozoites of the PyAPH-iKO parasite pretreated with RAP or DMSO were incubated with erythrocytes for 10 min at 37 °C with or without permeabilization with Triton X-100 (TritonX (+) or (−)), then labeled with a panel of antibodies against AMA1 (A) or MTRAP (C). Target proteins AMA1 and MTRAP are colored in red. MSP1 (green) and HSP70 (yellow) were counterstained. To observe more merozoites trapped on erythrocytes, parasites were also treated with cytochalasin D (CytD). Scale bar, 2 μm. Sum intensity (top) and secretion area (bottom) of signals for AMA1 (B) or MTRAP (D) of 5–10 merozoites were obtained by NIS-elements software and significant difference was examined by Mann-Whitney *U* test. (For interpretation of the references to colour in this figure legend, the reader is referred to the web version of this article.)

org/10.1016/j.parint.2021.102479.

Declaration of conflict of interest

None.

Acknowledgements

We thank J. Sattabongkot for anti-PbHSP70 antibody, A. Holder for anti-Py235 antibody, and T. J. Templeton for critical reading of the manuscript. This study was performed at the Joint Usage/Research Center on Tropical Disease, Institute of Tropical Medicine (NEKKEN), Nagasaki University, Japan. TI is a recipient of DC1 scholarship from the Japan Society for the Promotion of Science (JSPS). NC was supported by the leading program, Nagasaki University, Japan. This study was partly supported by grants from JSPS-KAKENHI (19H03461 to OK and 17J09408 and 20K22782 to TI) and the Japan Science Society (Sasakawa Scientific Research Grant 2020-4042 to TI). The funders have no role in the study design, data collection and analysis, decision to publish, or preparation of the manuscript.

References

[1] World Health Organization, World Malaria Report 2020, World Health Organization, Geneva, 2020, ISBN 978-92-4-001579-1.
[2] K. Yahata, M. Treeck, R. Culleton, T.W. Gilberger, O. Kaneko, Time-lapse imaging of red blood cell invasion by the rodent malaria parasite *Plasmodium yoelii*, PLoS One 7 (12) (2012), e50780, https://doi.org/10.1371/journal.pone.0050780.
[3] G.E. Weiss, P.R. Gilson, T. Taechalertpaisarn, W.H. Tham, N.W. de Jong, K. L. Harvey, F.J. Fowkes, P.N. Barlow, J.C. Rayner, G.J. Wright, A.F. Cowman, B. S. Crabb, Revealing the sequence and resulting cellular morphology of receptor-ligand interactions during *Plasmodium falciparum* invasion of erythrocytes, PLoS Pathog. 11 (2) (2015), e1004670, https://doi.org/10.1371/journal.ppat.1004670.
[4] A.F. Cowman, C.J. Tonkin, W.H. Tham, M.T. Duraisingh, The molecular basis of erythrocyte invasion by malaria parasites, Cell Host Microbe 22 (2) (2017) 232–245, https://doi.org/10.1016/j.chom.2017.07.003.
[5] K. Yahata, M.N. Hart, H. Davies, M. Asada, T.J. Templeton, M. Treeck, R.W. Moon, O. Kaneko, Gliding motility of *Plasmodium* merozoites, bioRxiv (2020), https://doi.org/10.1101/2020.05.01.072637.
[6] M.R. Galinski, C.C. Medina, P. Ingravallo, J.W. Barnwell, A reticulocyte-binding protein complex of *Plasmodium vivax* merozoites, Cell 69 (7) (1992) 1213–1226, https://doi.org/10.1016/0092-8674(92)90642-p.
[7] L.H. Miller, M. Aikawa, J.G. Johnson, T. Shiroishi, Interaction between cytochalasin B-treated malarial parasites and erythrocytes. Attachment and junction formation, J. Exp. Med. 149 (1) (1979) 172–184, https://doi.org/10.1084/jem.149.1.172.
[8] Y. Kegawa, M. Asada, T. Ishizaki, K. Yahata, O. Kaneko, Critical role of erythrocyte binding-like protein of the rodent malaria parasite *Plasmodium yoelii* to establish an irreversible connection with the erythrocyte during invasion, Parasitol. Int. 67 (6) (2018) 706–714, https://doi.org/10.1016/j.parint.2018.07.006.
[9] D.L. Alexander, J. Mital, G.E. Ward, P. Bradley, J.C. Boothroyd, Identification of the moving junction complex of *Toxoplasma gondii*: a collaboration between distinct secretory organelles, PLoS Pathog. 1 (2) (2005), e17, https://doi.org/10.1371/journal.ppat.0010017.
[10] D.T. Riglar, D. Richard, D.W. Wilson, M.J. Boyle, C. Dekiwadia, I. Turnbull, F. Angrisano, D.S. Marapana, K.L. Rogers, C.B. Whitchurch, J.G. Beeson, A. F. Cowman, S.A. Ralph, J. Baum, Super-resolution dissection of coordinated events during malaria parasite invasion of the human erythrocyte, Cell Host Microbe 9 (1) (2011) 9–20, https://doi.org/10.1016/j.chom.2010.12.003.
[11] S. Besteiro, J.F. Dubremetz, M. Lebrun, The moving junction of apicomplexan parasites: a key structure for invasion, Cell. Microbiol. 13 (6) (2011) 797–805, https://doi.org/10.1111/j.1462-5822.2011.01597.x.
[12] J.A. Dvorak, L.H. Miller, W.C. Whitehouse, T. Shiroishi, Invasion of erythrocytes by malaria merozoites, Science. 187 (4178) (1975) 748–750, https://doi.org/10.1126/science.803712.
[13] P.R. Gilson, B.S. Crabb, Morphology and kinetics of the three distinct phases of red blood cell invasion by *Plasmodium falciparum* merozoites, Int. J. Parasitol. 39 (1) (2009) 91–96, https://doi.org/10.1016/j.ijpara.2008.09.007.
[14] D.J. Dubois, D. Soldati-Favre, Biogenesis and secretion of micronemes in *Toxoplasma gondii*, Cell. Microbiol. 21 (5) (2019), e13018, https://doi.org/10.1111/cmi.13018.
[15] H.E. Bullen, Y. Jia, Y. Yamaryo-Botte, H. Bisio, O. Zhang, N.K. Jemelin, J.B. Marq, V. Carruthers, C.Y. Botte, D. Soldati-Favre, Phosphatidic acid-mediated signaling regulates microneme secretion in *Toxoplasma*, Cell Host Microbe 19 (3) (2016) 349–360, https://doi.org/10.1016/j.chom.2016.02.006.
[16] N. Darvill, D.J. Dubois, S.L. Rouse, P.M. Hammoudi, T. Blake, S. Benjamin, B. Liu, D. Soldati-Favre, S. Matthews, Structural basis of phosphatidic acid sensing by APH in *Apicomplexan parasites*, Structure 26 (8) (2018) 1059–1071, https://doi.org/10.1016/j.str.2018.05.001.
[17] A. Farrell, S. Thirugnanam, A. Lorestani, J.D. Dvorin, K.P. Eidell, D.J. Ferguson, B. R. Anderson-White, M.T. Duraisingh, G.T. Marth, M.J. Gubbels, A DOC2 protein identified by mutational profiling is essential for apicomplexan parasite exocytosis, Science 335 (6065) (2012) 218–221, https://doi.org/10.1126/science.1210829.
[18] X. Gao, K. Gunalan, S.S. Yap, P.R. Preiser, Triggers of key calcium signals during erythrocyte invasion by *Plasmodium falciparum*, Nat. Commun. 4 (2013) 2862, https://doi.org/10.1038/ncomms3862.
[19] Z. Ebrahimzadeh, A. Mukherjee, M.E. Crochetiere, A. Sergerie, S. Amiar, L. A. Thompson, D. Gagnon, D. Gaumond, R.V. Stahelin, J.B. Dacks, D. Richard, A pan-apicomplexan phosphoinositide-binding protein acts in malarial microneme exocytosis, EMBO Rep. 20 (6) (2019), https://doi.org/10.15252/embr.201847102 e47102.
[20] H.E. Bullen, D. Soldati-Favre, A central role for phosphatidic acid as a lipid mediator of regulated exocytosis in apicomplexa, FEBS Lett. 590 (15) (2016) 2469–2481, https://doi.org/10.1002/1873-3468.12296.
[21] S. Yeoh, R.A. O'Donnell, K. Koussis, A.R. Dluzewski, K.H. Ansell, S.A. Osborne, F. Hackett, C. Withers-Martinez, G.H. Mitchell, L.H. Bannister, J.S. Bryans, C. A. Kettleborough, M.J. Blackman, Subcellular discharge of a serine protease mediates release of invasive malaria parasites from host erythrocytes, Cell 131 (6) (2007) 1072–1083, https://doi.org/10.1016/j.cell.2007.10.049.
[22] J.K. Mutungi, K. Yahata, M. Sakaguchi, O. Kaneko, Isolation of invasive *Plasmodium yoelii* merozoites with a long half-life to evaluate invasion dynamics and potential invasion inhibitors, Mol. Biochem. Parasitol. 204 (1) (2015) 26–33, https://doi.org/10.1016/j.molbiopara.2015.12.003.
[23] T. Ishizaki, M. Asada, H. Hakimi, N. Chaiyawong, Y. Kegawa, K. Yahata, O. Kaneko, cAMP-dependent protein kinase regulates secretion of apical membrane antigen 1 (AMA1) in *Plasmodium yoelii*, Parasitol. Int. 85 (2021) 102435, https://doi.org/10.1016/j.parint.2021.102435.
[24] T. Ishizaki, N. Chaiyawong, H. Hakimi, M. Asada, M. Tachibana, T. Ishino, K. Yahata, O. Kaneko, A novel *Plasmodium yoelii* pseudokinase, PypPK1, is involved in erythrocyte invasion and exflagellation center formation, Parasitol. Int. 76 (2020) 102056, https://doi.org/10.1016/j.parint.2020.102056.
[25] M.L. Jones, S. Das, H. Belda, C.R. Collins, M.J. Blackman, M. Treeck, A versatile strategy for rapid conditional genome engineering using loxP sites in a small synthetic intron in *Plasmodium falciparum*, Sci. Rep. 6 (2016) 21800, https://doi.org/10.1038/srep21800.
[26] R.Y. Orr, N. Philip, A.P. Waters, Improved negative selection protocol for *Plasmodium berghei* in the rodent malaria model, Malar. J. 11 (2012) 103, https://doi.org/10.1186/1475-2875-11-103.
[27] J.K. Mutungi, K. Yahata, M. Sakaguchi, O. Kaneko, Expression and localization of rhoptry neck protein 5 in merozoites and sporozoites of *Plasmodium yoelii*, Parasitol. Int. 63 (6) (2014) 794–801, https://doi.org/10.1016/j.parint.2014.07.013.
[28] H. Otsuki, O. Kaneko, A. Thongkukiatkul, M. Tachibana, H. Iriko, S. Takeo, T. Tsuboi, M. Torii, Single amino acid substitution in *Plasmodium yoelii* erythrocyte ligand determines its localization and controls parasite virulence, Proc. Natl. Acad. Sci. U. S. A. 106 (2009) 7167–7172, https://doi.org/10.1073/pnas.0811313106.
[29] H.K. Bayele, K.N. Brown, Delineation of epitopes on the Py235 rhoptry antigen of *Plasmodium yoelii* YM, FEMS Immunol. Med. Microbiol. 50 (3) (2007) 389–395, https://doi.org/10.1111/j.1574-695X.2007.00269.x.
[30] R.S. Kent, K.K. Modrzynska, R. Cameron, N. Philip, O. Billker, A.P. Waters, Inducible developmental reprogramming redefines commitment to sexual development in the malaria parasite *Plasmodium berghei*, Nat. Microbiol. 3 (11) (2018) 1206–1213, https://doi.org/10.1038/s41564-018-0223-6.
[31] M. Tsuji, D. Mattei, R.S. Nussenzweig, D. Eichinger, F. Zavala, Demonstration of heat-shock protein 70 in the sporozoite stage of malaria parasites, Parasitol. Res. 80 (1994) 16–21, https://doi.org/10.1007/BF00932618.
[32] B.F. Kafsack, J.D. Pena, I. Coppens, S. Ravindran, J.C. Boothroyd, V.B. Carruthers, Rapid membrane disruption by a perforin-like protein facilitates parasite exit from host cells, Science 323 (5913) (2009) 530–533, https://doi.org/10.1126/science.1165740.
[33] D.Y. Bargieri, S. Thiberge, C.L. Tay, A.F. Carey, A. Rantz, F. Hischen, A. Lorthiois, U. Straschil, P. Singh, S. Singh, T. Triglia, T. Tsuboi, A. Cowman, C. Chitnis, P. Alano, J. Baum, G. Pradel, C. Lavazec, R. Menard, *Plasmodium* merozoite TRAP family protein is essential for vacuole membrane disruption and gamete egress from erythrocytes, Cell Host Microbe 20 (5) (2016) 618–630, https://doi.org/10.1016/j.chom.2016.10.015.
[34] R.E. Cooke, S. Moore, L.F. Anderson, C.J. Janse, A.P. Waters, PTRAMP; a conserved *Plasmodium thrombospondin*-related apical merozoite protein, Mol. Biochem. Parasitol. 134 (2) (2004) 225–232, https://doi.org/10.1016/j.molbiopara.2003.12.003.
[35] M. Zhang, C. Wang, T.D. Otto, J. Oberstaller, X. Liao, S.R. Adapa, K. Udenze, I. F. Bronner, D. Casandra, M. Mayho, J. Brown, S. Li, J. Swanson, J.C. Rayner, R.H. Y. Jiang, J.H. Adams, Uncovering the essential genes of the human malaria parasite *Plasmodium falciparum* by saturation mutagenesis, Science 360 (6388) (2018) eaap7847, https://doi.org/10.1126/science.aap7847.
[36] C. Aurrecoechea, J. Brestelli, B.P. Brunk, J. Dommer, S. Fischer, B. Gajria, X. Gao, A. Gingle, G. Grant, O.S. Harb, M. Heiges, F. Innamorato, J. Iodice, J.C. Kissinger, E. Kraemer, W. Li, J.A. Miller, V. Nayak, C. Pennington, D.F. Pinney, D.S. Roos, C. Ross, C.J. Jr Stoeckert, C. Treatman, H. Wang, PlasmoDB: a functional genomic database for malaria parasites, Nucleic Acids Res. 37 (2009) D539–D543, https://doi.org/10.1093/nar/gkn814.